THE PROTEIN SOCIETY

Effects of ligand binding on the stability of aldo–keto reductases: Implications for stabilizer or destabilizer chaperones

Aurangazeb Kabir,[1] Ryo P. Honda,[2] Yuji O. Kamatari,[3] Satoshi Endo,[4] Mayuko Fukuoka,[1] and Kazuo Kuwata[1,5]*

[1]United Graduate School of Drug Discovery and Medical Information Sciences, Gifu University, Gifu 501-1193, Japan
[2]Department of Molecular Pathobiochemistry, Graduate School of Medicine, Gifu University, Gifu 501-1193, Japan
[3]Life Science Research Center, Gifu University, Gifu 501-1193, Japan
[4]Laboratory of Biochemistry, Gifu Pharmaceutical University, Gifu 501-1196, Japan
[5]Department of Gene and Development, Graduate School of Medicine, Gifu University, Gifu 501-1193, Japan

Received 6 June 2016; Accepted 30 August 2016
DOI: 10.1002/pro.3036
Published online 6 September 2016 proteinscience.org

Abstract: Ligands such as enzyme inhibitors stabilize the native conformation of a protein upon binding to the native state, but some compounds destabilize the native conformation upon binding to the non-native state. The former ligands are termed "stabilizer chaperones" and the latter ones "destabilizer chaperones." Because the stabilization effects are essential for the medical chaperone (MC) hypothesis, here we have formulated a thermodynamic system consisting of a ligand and a protein in its native- and non-native state. Using the differential scanning fluorimetry and the circular dichroism varying the urea concentration and temperature, we found that when the coenzyme $NADP^+$ was absent, inhibitors such as isolithocholic acid stabilized the aldo–keto reductase AKR1A1 upon binding, which showed actually the three-state folding, but destabilized AKR1B10. In contrast, in the presence of $NADP^+$, they destabilized AKR1A1 and stabilized AKR1B10. To explain these phenomena, we decomposed the free energy of stabilization ($\Delta\Delta G$) into its enthalpy ($\Delta\Delta H$) and entropy ($\Delta\Delta S$) components. Then we found that in a relatively unstable protein showing the three-state folding, native conformation was stabilized by the negative $\Delta\Delta H$ in association with the negative $\Delta\Delta S$, suggesting that the stabilizer chaperon decreases the conformational fluctuation of the target protein or increase its hydration. However, in other cases, $\Delta\Delta G$ was essentially determined by the delicate balance between $\Delta\Delta H$ and $\Delta\Delta S$. The proposed thermodynamic formalism is applicable to the system including multiple ligands with allosteric interactions. These findings would promote the development of screening strategies for MCs to regulate the target conformations.

Keywords: medical chaperone; stabilizer; destabilizer; entropy; protein conformation; aldo–keto reductase; $\Delta\Delta G$; $\Delta\Delta S$

Additional Supporting Information may be found in the online version of this article.

Grant sponsor: The Ministry of Education, Culture, Sports, Science and Technology of Japan (K. K.); Grant sponsor: The Ministry of Health, Labour and Welfare; Grant sponsor: Practical Research Project for Rare/Intractable Disease of the Japan Agency for Medical Research Development (AMED).

*Correspondence to: Kazuo Kuwata; United Graduate School of Drug Discovery and Medical Information Sciences, Gifu University, Yanagido 1-1, Gifu 501-1193, Japan. E-mail: kuwata@gifu-u.ac.jp

Introduction

Medical chaperones (MCs)[1–4] are small molecules capable of modulating the free energy landscape of a protein upon binding, thereby increasing the stability of the native conformation and preventing the abnormal aggregate formation. Although MCs are considered to be the candidates of therapeutic agents for treating various conformational diseases,[1–4] the general formulation of their mechanism of action or concrete experimental evidence showing the degree of stabilization have not yet been described. Here we propose the thermodynamic formulation of the stabilization effects on protein conformations upon ligand binding, and also provide the experimental evidences for the proposed formalism using aldo–keto reductases (AKR) superfamily proteins.

AKR superfamily[5,6] was extensively studied as a target for anti-cancer drug design.[7,8] Especially AKR1B10 was reported to be closely associated with cell carcinogenesis and tumor development by regulating the retinoid acid homeostasis,[5,6] the lipid metabolism,[9] and the isoprenoid metabolism.[10] For AKR superfamily, various ligands were synthesized[11,12] and their interactions were extensively studied.[10] Hence, AKR superfamily was considered to be the appropriate system to examine the proposed formalism.

To describe the ligand binding to the protein, population of the denatured state is not negligible, as the Gibbs free energy difference (ΔG) between the denatured (D) and native state (N) is usually < 10 kcal/mol,[13] and the ligand binding may markedly perturb ΔG, affecting the population of N. Therefore in order to discuss the stability of the native conformation, here we introduce ligand (L), N, intermediate state (I) and D into the physical model described by the following scheme;

$$D + L \leftrightarrow N + L \leftrightarrow I + L \leftrightarrow IL \leftrightarrow NL \text{ (Scheme 1)},$$

in which N and NL are considered to be within the native ensemble in the presence of L, while I, IL, and D are within the non-native ensemble. DL may be eliminated in case of MCs because of their specific interaction with the well-defined binding pockets.

Under the above perspective, the ligand can perturb the stability of the native state with the free energy of stabilization ($\Delta\Delta G$) as illustrated in Figure 1, whose sign is either negative [Fig. 1(A)] or positive [Fig. 1(B)]. The native conformation is stabilized in the presence of a ligand (stabilizer chaperone) [Fig. 1(A)] or destabilized (destabilizer chaperone) [Fig. 1(B)]. Here we present several experimental examples of stabilizer and destabilizer chaperones demonstrated by the differential scanning fluorimetry (DSF),[14] and the circular dichroism (CD) as a function of denaturant concentration and temperature.

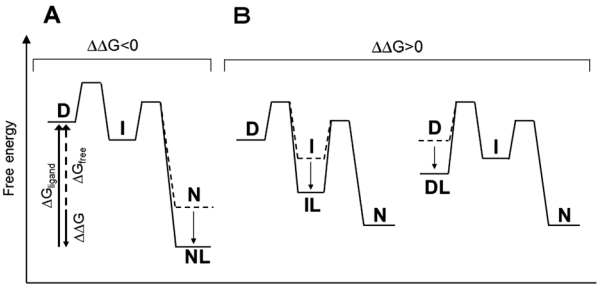

Figure 1. Possible mechanisms for the (de)stabilization of the native state by ligands. The ligand binding to different states results in different thermodynamic effects on proteins. (A) The ligand preferentially binds to the native state (*N*), which results in the stabilization of the native state ($\Delta\Delta G < 0$). (B) The ligand preferentially binds to an intermediate state (*I*) or the denatured state (*D*), which results in the destabilization of the native state ($\Delta\Delta G > 0$). Note that $\Delta\Delta G = \Delta G_{free} - \Delta G_{ligand}$.

By the nonlinear curve fitting, we also decomposed $\Delta\Delta G$ into the enthalpy contribution ($\Delta\Delta H$), and the entropy contribution ($\Delta\Delta S$), which depends on the characteristics of the conformational fluctuation of the protein and/or the solvation,[15] and finally discussed on the overall thermodynamic pictures of the stabilizer- and the destabilizer chaperones.

Results

Effects of isolithocholic acid on the stability of AKR superfamily proteins

The melting temperature (T_m) of AKR1A1[16] [Fig. 2(A)] decreased with increasing concentration of isolithocholic acid (ILCA) in the presence of coenzyme $NADP^+$, as shown in Figure 2(C). However, T_m of AKR1B10[17] [Fig. 2(B)] increased with increasing concentration of ILCA, as shown in Figure 2(D). Thus, in the presence of $NADP^+$, ILCA destabilized AKR1A1, but stabilized AKR1B10.

Next, we surveyed T_m for 24 combinations of six compounds (C9, C26, C18, C21, C12, and C14) and two proteins (AKR1A1 and AKR1B10) in the presence or absence of $NADP^+$ (Fig. 3). The difference in T_m upon binding of ligands (ΔT_m) varies depending on the combination of ligand, protein, and $NADP^+$. However, ΔT_m values were almost all positive, indicating the stabilizing effect on AKR1s, except for the combination of ILCA and AKR1A1 shown in Figure 3(D).

According to the thermodynamic formulation on the change in stability of the conformation upon ligand binding shown in the Eq. (A15) in Appendix, $\Delta\Delta G$ is linearly dependent on temperature upon binding in the experimental condition where $T \sim T_m$ (See Appendix for definitions of variables.).

$$\frac{\Delta\Delta G}{T} \sim -\Delta\Delta S + \Delta C_{p,D-N(T)}\left(\Delta T + \ln\left(\frac{T_m^b}{T_m^0}\right)\right) \quad (1)$$

We measured the T_m of a lysozyme solution as a function of urea or guanidine hydrochloride. As

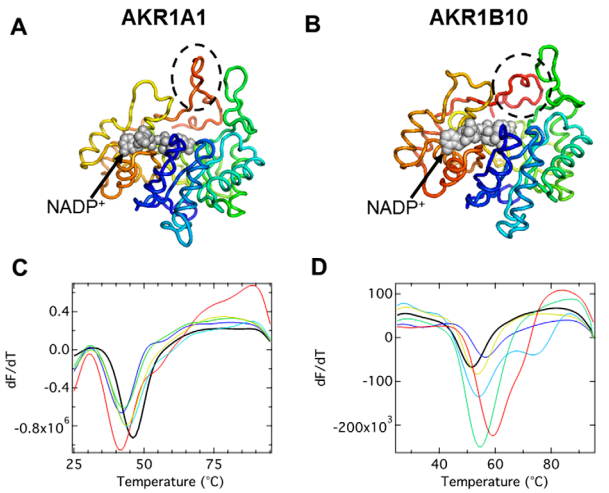

Figure 2. (A) Three-dimensional (3D) structure of AKR1A1 in complex with $NADP^+$ (PDB: 2ALR[16]). (B) 3D structure of AKR1B10 in complex with $NADP^+$ (PDB: 1ZUA[17]). A key structural difference between AKR1B10 and AKR1A1 lies in a loop region at the N-terminus, which is indicated by the dotted circle. (C) Differential scanning fluorimetry (DSF) curves of AKR1A1 in the presence of various concentrations of C21 [Isolithocholic acid (ILCA), 0 (black), 3.13 (yellow), 6.25 (light blue), 12.5 (green), 25 (blue), and 50 (red) μM]. (D) DSF curves of AKR1B10 in the presence of various concentrations of C21 [0 (black), 3.13 (yellow), 6.25 (light blue), 12.5 (green), 25 (blue), and 50 (red) μM].

shown in Figure S1 (Supporting Information), T_m decreased almost linearly with increase in the urea or guanidine hydrochloride concentration. As the free energy of the protein solution is linearly dependent on the denaturant concentration,[18] this clearly indicates that Eq. (1) is valid within the observed temperature scale.

We used SYPRO Orange for the fluorescence detection in DSF, but it binds to the intermediate state or the denatured state of a protein, and thus destabilizes the native conformation. To remove this effect of SYPRO Orange, we used the difference in the melting temperature (ΔT_m). However, to confirm the above phenomena further and to analyze the effects of ligand binding more quantitatively, we used CD spectra as a function of temperature and urea concentration, applied the proposed formalism to the AKR and inhibitor system, and evaluated $\Delta\Delta G$, $\Delta\Delta H$, and $\Delta\Delta S$ upon ligand binding.

Stabilization of AKR1A1 by ligand binding in the absence of NADP$^+$

We measured the urea denaturation curve of AKR1A1 in the absence of coenzyme $NADP^+$ using CD spectra [Fig. S2(A), Supporting Information; 4(A)]. Surprisingly, during the folding process of AKR1A1, a folding intermediate was clearly observed [Fig. 4(A), red], indicating that the process involves at least three states. Native, intermediate, and denatured populations were obtained by fitting of the CD denaturation curves as a function of urea concentration [Fig. S2(C), Supporting Information]. Conversely, in the presence of ILCA, the native conformation was markedly stabilized, as shown in Figure S2(B) and S2(D), Supporting Information. AKR1A1 was stabilized by the binding of ligands such as C18 or C21 (ILCA) [Fig. 4(A)], and also strongly stabilized by the binding of $NADP^+$ [Fig. 4(B)]. To understand the thermodynamic origin of the stability, we next decomposed the free energy of stabilization into the enthalpy- and the entropy components using a previously described method.[19,20] Briefly, we measured urea-denaturation at various temperature (5–35°C) in the presence or absence of ligands, to obtain the temperature dependence of ΔG. The ΔG versus temperature plot was subsequently fit to Gibbs–Helmholtz equation [Eq. (2)] to calculate the ΔS and ΔH contributions to the ΔG. The $\Delta\Delta H$ and $\Delta\Delta S$ were then calculated using the Eqs. (5) and (6), and plotted in Figure 5(A). Notably, entropy decreased upon the binding of C18 and C21 to AKR1A1 ($\Delta\Delta S < 0$).

Destabilization of AKR1A1 by ligand binding in the presence of NADP$^+$

Next, we performed a similar analysis in the presence of $NADP^+$. Intriguingly, the folding reaction of AKR1A1 almost showed a two-state process in the presence of $NADP^+$ [red line in Fig. 4(B)]. Moreover,

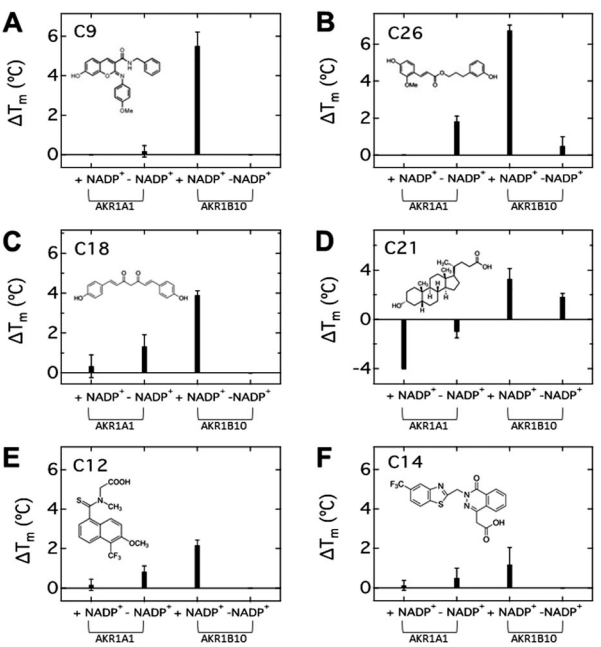

Figure 3. Changes in melting temperature (ΔT_m) of AKR1A1 and AKR1B10 in the presence and the absence of $NADP^+$ with C9 (A), C26 (B), C18 (C), C21 (D), C12 (E) and C14 (F), which are considered as potential inhibitors of human aldo–keto reductases familie members (AKR1).

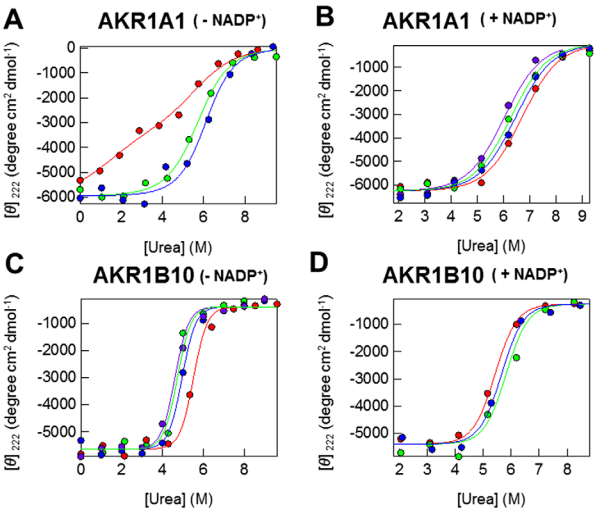

Figure 4. The thermal stability of AKR1A1 and AKR1B10 measured using far-UV CD. Measurements were performed at 5°C in the presence and absence of various compounds. (A) AKR1A1 in the absence of $NADP^+$. The molar ellipticities as a function of urea in the absence of ligand (red circles) or in the presence of C18 (green circles), or C21 (blue circles) are shown. (B) AKR1A1 in the presence of $NADP^+$. The molar ellipticities as a function of urea in the absence of ligand (red circles) or in the presence of C12 (purple circles), C18 (green circles), or C21 (blue circles) are shown. (C) AKR1B10 in the absence of $NADP^+$. The molar ellipticities as a function of urea in the absence of ligand (red circles) or in the presence of C18 (blue circles), C21 (purple circles), or C26 (green circles) are shown. (D) AKR1B10 in the presence of $NADP^+$. The molar ellipticities as a function of urea in the absence of ligand (red circles) or in the presence of C21 (purple circles) or C26 (green circles) are shown. The solid lines represent least-square fits to three-state or two-state unfolding equations.

the binding of ligands such as C12, C18, or C21 destabilized the native conformation of AKR1A1 [Fig. 4(B)]. The positive $\Delta\Delta G$ values depend on the delicate balance of entropy- and enthalpy contribution, as shown in Figure 5(B).

Destabilization of AKR1B10 in the absence of $NADP^+$

We measured the urea denaturation curve of AKR1B10 in the absence of the coenzyme $NADP^+$ using CD spectra [Fig. 4(C)]. AKR1B10 showed a clear two-state transition. Conversely, in the presence of C18, C21 (ILCA), and C26, the native conformation was markedly destabilized, as shown in Figure 4(C). The temperature dependence of ΔG was obtained using the curve fitting of $[\Theta]_{222}$ as described above, and the obtained $\Delta\Delta S$ and $\Delta\Delta H$ contributions are plotted in Figure 5(C). Notably, entropy increased upon the binding of C18, C21, and C26 ($\Delta\Delta S > 0$).

Stabilization of AKR1B10 in the presence of $NADP^+$

We conducted a similar analysis for AKR1B10 in the presence of $NADP^+$. The folding reaction of AKR1B10 was shown to have two-state characteristics in the presence of $NADP^+$ [Fig. 4(D)]. Intriguingly, the binding of ligands such as C21 and C26 stabilized the native state of AKR1B10 [Fig. 4(D)]. $\Delta\Delta G$ decreased upon binding of C21 and C26 [Fig. 5(D)], and $\Delta\Delta S$ values were positive.

Discussion

The key and lock model or induced fit model[21] was used to describe the interaction between a protein and a ligand, enabling the determination of the free energy of binding. However, this approach never explains the stability of the native conformation or $\Delta\Delta G$, because the denatured state is not included in the model. Historically the effect of ligands on protein stability was investigated using calorimetry[22,23] and the spectroscopic methods.[24,25] Recently, coupled folding-binding reaction was reported on the intrinsically disordered protein.[26,27] The idea of stabilization of the native state by ligand binding was qualitatively described,[28] and the quantitative formulation and its numeric solution were recently proposed.[25]

Here we have shown that ILCA stabilizes the native state of AKR1A1 in the absence of $NADP^+$, while destabilizes the native state of AKR1A1 in the presence of $NADP^+$. Conversely, ILCA destabilizes the native state of AKR1B10 in the absence of $NADP^+$, while stabilizes the native state of AKR1B10

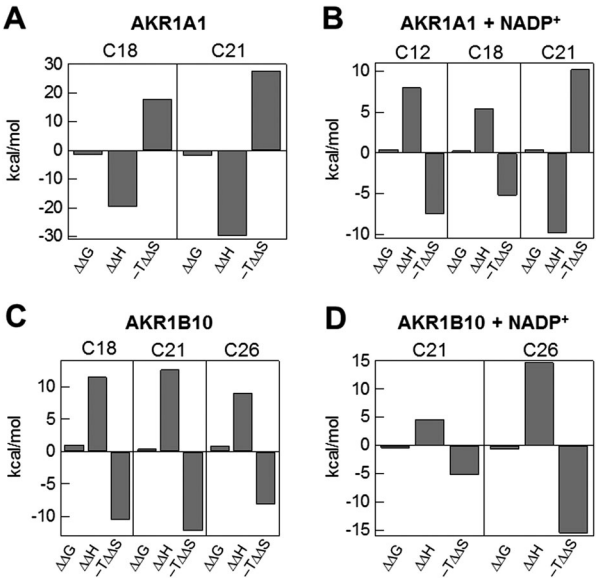

Figure 5. Thermodynamic profiles at 20°C ($\Delta\Delta G$, $\Delta\Delta H$, and $-T\Delta\Delta S$) of the ligand binding to (A) AKR1A1 in the presence of $NADP^+$, (B) AKR1A1 in the absence of $NADP^+$, (C) AKR1B10 in the presence of $NADP^+$, and (D) AKR1B10 in the absence of $NADP^+$.

in the presence of $NADP^+$. Binding site of $NADP^+$ was already elucidated[16,17] and the binding site of Tolrestat (C12) was different than that of $NADP^+$. Thus those interactions are considered to be the allosteric effect.[27,29,30] The structure of AKR1A1[16] is slightly different from that of AKR1B10[17] in the region indicated by the dotted circle in Figure 2(A) and (B). AKR1A1 forms a β-sheet, whereas AKR1B10 forms a loop, both of which are somewhat close to the $NADP^+$-binding site. Although the structures near the catalytic site differ between the two proteins, the differences in their interactions with ligands remain elusive.

In order to treat these complex systems, we need to establish a general scheme in which the interaction with more than one ligand and the conformational change of a protein upon ligand binding are allowed.

We here propose a simple thermodynamic model system as described in Appendix, which is generally applicable to the system including the non-native- or denatured state to yield $\Delta\Delta G$ upon binding of a ligand using the equilibrium binding constants (K_{dN} and K_{dI}) or the general thermodynamic parameters (see Appendix).

In order to decompose $\Delta\Delta G$ into $\Delta\Delta H$ and $\Delta\Delta S$ contributions, here we also included the ΔC_p contribution in the analysis shown in Eqs. (1–4), and found that to stabilize the relatively unstable native state ($\Delta\Delta G < 0$), it might be important to reduce the conformational fluctuation ($\Delta\Delta S < 0$) with the expense of $\Delta\Delta H$ (> 0), as shown in Figure 5(A), while in other case, the sign of $\Delta\Delta G$ generally depends on the delicate balance of $\Delta\Delta S$ and $\Delta\Delta H$, as shown in Figure 5(B–D), and Table I. Of note, as shown in Table I, ΔC_p and m values were distinct but similar between different protein systems.

High energy states[4,31] usually associated with the ligand binding were reported to be within the native ensemble, and the bound state is considered to be different than the unbound state. However, as long as these multiple states are within the native ensemble, they may increase overall stability of the native ensemble. Whereas these states are outside of the native ensemble, they will decrease the stability of the native ensemble.

Therefore, the ligands that stabilize the native state ($\Delta\Delta G < 0$) [Fig. 1(A)] bind primarily to the native conformation (N), while those destabilize the native state ($\Delta\Delta G > 0$) bind to the intermediate (I) or denatured state (D) [Fig. 1(B)]. In this viewpoint, it is intriguing that in the absence of $NADP^+$, ligands mainly bind to the native AKR1A1 and to the intermediate or the denatured state of AKR1B10, while in the presence of $NADP^+$, ligands mainly bind to the intermediate or the denatured state of AKR1A1 and to the native AKR1B10, as shown in Figure 4. Although ligand binding to denatured state[25,32] of other proteins were reported, in AKRs there is no structural evidence for the binding to the non-native or denatured state at this stage and their native structures are actually similar [Fig. 2(A,B)]. However, because the homology of aminoacid sequences of AKR1A1[33] and AKR1B10[34] is 51.5%, ligand-binding properties of their denatured states may be somewhat different. It must be emphasized again that $\Delta\Delta G$ depends on the subtle balance between ΔH and ΔS and also between the binding constants with native, intermediate, and denatured states.

ILCA may bind to the intermediate state of AKR1A1 with $NADP^+$ [Fig. 4(B)] where binding pocket may be at least conserved, but this state has not been directly observed. Although bile acids are reported to induce protein unfolding,[35] here it was shown that ILCA stabilizes the native conformation of AKR1A1 without $NADP^+$ [Fig. 4(A)]. It is interesting to note that lithocholic acid inhibits the polymerization of PiZ alpha-1-antitrypsin,[36] and extends the life span of the yeast *Saccharomyces cerevisiae*.[37] The variety of functions of lithocholic acids may be arose from their action on the wide spectrum of the protein conformation.

A thermodynamic study on the stabilization of α-galactosidase upon binding of a pharmacological chaperone was reported.[38] It was also reported that the aggregation of α-galactosidase is a determinant of its efficacy against Fabry disease.[39] Therefore, stabilization of the native conformation of proteins is an important strategy to prevent the diseases associated with protein misfolding. However, many reports on the small compounds have emphasized their stabilization effects on the native conformations thus far. In fact, during the *in silico* screening process of anti-prion compounds, we eventually found that many compounds inhibited pathogenic conversion, although some compounds promoted the pathogenic conversion reaction.[40] Small compounds that stabilize the native conformation of a prion protein may be regarded as stabilizer chaperones, whereas compounds that destabilize the prion protein and promote conversion reaction may be regarded as destabilizer chaperones. Thus an important goal is to establish a rational strategy to design stabilizer or destabilizer chaperones depending on the target proteins. For instance, to prevent the aggregate formation, we may stabilize either native-, intermediate-, or even denatured state depending on the conformational properties of the target protein.

Materials and Methods

Materials

Dimethylsulfoxide (DMSO), methanol, $NADP^+$, and the fluorescent dye used in the DSF experiments, as well as SYPRO® Orange Protein Gel Stain (supplied as S5692) were obtained from Sigma-Aldrich Co.

Table I. *Summary of Ligand-Binding Properties*

Protein	System	Ligand	IC_{50} (nM)	T_m[b] (°C)	ΔH_{vf}[c] (kcal/mol)	ΔC_p[c] (kcal/mol K)	m-value[d] (kcal/mol M)	ΔH[e] [$\Delta\Delta H$] (kcal/mol)	$-T\Delta S$[e] [$-T\Delta\Delta S$] (kcal/mol)	ΔG[e] [$\Delta\Delta G$] (kcal/mol)
AKR1A1	3-state (U↔I↔N)	none	-	46.5 ± 0.4	106.7 ± 6.0	4.10 ± 0.33	0.98 ± 0.06	−1.86 [-]	6.07 [-]	4.21 [-]
		C18	N.D.[a]	46.6 ± 0.5	126.7 ± 6.0			17.78 [−19.64]	−11.90 [17.97]	5.88 [−1.66]
		C21	N.D.[a]	45.0 ± 1.1	130.3 ± 5.9			27.91 [−29.77]	−21.80 [27.88]	6.11 [−1.89]
AKR1A1 + $NADP^+$	2-state (U↔N)	none	-	45.7 ± 0.3	114.5 ± 4.0	3.63 ± 0.22	0.79 ± 0.01	21.52 [-]	−16.13 [-]	5.39 [-]
		C12	42,000	46.1 ± 0.3	108.3 ± 3.8			13.46 [8.06]	−8.59 [−7.54]	4.87 [0.52]
		C18	2,900	46.1 ± 0.3	110.8 ± 4.0			15.99 [5.53]	−10.92 [−5.21]	5.07 [0.32]
		C21	68,000	42.1 ± 0.1	111.6 ± 4.0			31.35 [−9.83]	−26.40 [10.28]	4.94 [0.45]
AKR1B10	2-state (U↔N)	none	-	52.6 ± 0.1	149.4 ± 3.1	3.64 ± 0.14	1.65 ± 0.04	30.76 [-]	−21.95 [-]	8.81 [-]
		C18	N.D.[a]	52.8 ± 0.1	138.6 ± 3.1			19.21 [11.55]	−11.49 [−10.47]	7.73 [1.08]
		C21	N.D.[a]	54.7 ± 0.1	140.7 ± 3.2			18.04 [12.72]	−9.69 [−12.26]	8.34 [0.46]
		C26	N.D.[a]	52.7 ± 0.1	144.3 ± 3.1			21.7 [9.05]	−13.77 [−8.18]	7.94 [0.87]
AKR1B10+ $NADP^+$	2-state (U↔N)	none	-	54.0 ± 0.4	122.2 ± 2.8	2.79 ± 0.13	1.43 ± 0.04	27.36 [-]	−19.77 [-]	7.59 [-]
		C21	27	56.9 ± 0.1	125.5 ± 3.2			22.67 [4.72]	−14.61 [−5.19]	8.06 [−0.47]
		C26	6.2	61.0 ± 0.1	126.9 ± 2.9			12.57 [14.82]	−4.32 [−15.48]	8.25 [−0.66]

[a] IC_{50} value was not determined, because the enzymatic activity is absent without the cofactor, $NADP^+$.
[b] Melting temperature obtained by DSF experiments. Error represents the standard deviation in three experiments.
[c] Van't Hoff enthalpy and heat capacity obtained by analyzing the ΔG versus T plot over 5°C −35°C (see Material and Methods section). Error represents the fitting error in one S.D.
[d] m-value in the transition from the unfolded to native states, obtained by urea-unfolding experiments. Error represents the fitting error in one S.D.
[e] Enthalpic and entropic contributions to the free energy at 20°C, which were calculated from the T_m, ΔC_p and ΔH_{vf} on the basis of the Eqs. (3) and (4).

LLC. (St. Louis, MO). SYPRO Orange was supplied as a DMSO solution at 5000× concentration. The buffer Gibco® PBS 1× pH 7.2 was purchased from Thermo Fisher Scientific Co. (Waltham MA). The compounds C9 [7-hydroxy-2-(4-methoxyphenylimino)−2*H*-chromene-3-carboxylic acid benzylamide)][11] and C26 [3-(4-hydroxy-2-methoxyphenyl)acrylic acid 3-(3-hydroxyphenyl)propyl ester)][12] were synthesized as previously described. C12 (Tolrestat), C14 (Zopolrestat), and C17 (Fidarestat) were kindly donated by Dr. P.F. Kador (University of Nebraska Medical Center). C18 (bisdemethoxycurcumin) was obtained from Nagara Science Co. (Gifu, Japan). Other reagents were purchased from Wako Pure Chemical Industries (Osaka, Japan).

Preparation of recombinant enzymes

Recombinant AKR1A1 and AKR1B10 with the N-terminal 6-His tag[10] were expressed in *Escherichia coli* cells harboring their cDNAs, and purified to homogeneity, as previously described.

Differential scanning fluorimetry

SYPRO Orange is an environmentally sensitive dye. The unfolding process exposes the hydrophobic region of proteins and results in a large increase in fluorescence, which is used to monitor the protein-unfolding transition. DSF was performed using the Applied Biosystems® StepOnePlus™ Real-Time PCR System [Thermo Fisher Scientific Co.], The SYBR green melting curve protocol was followed in each experiment to obtain the T_m with this PCR system machine. Initially, the general procedure outlined by Nielsen *et al*. was followed.[41]

We tested six compounds (C9, C26, C18, C21, C12, and C14) for AKR superfamily proteins. C9 (0.8 m*M*) and the other compounds (1 m*M*) were dissolved in DMSO/methanol (1:9v/v) and in methanol, respectively. In a single well of a 96-well PCR plate (Ultra Amp PCR plates; Sorenson, BioScience, Murray, UT), a 20-μL reaction solution was placed in each well prepared by mixing 4 μL of protein solution, 4 μL of 20× SYPRO Orange (diluted from 5000× stock in DMSO), 0.5 μL of the compound, 10.5 μL of buffer solution (phosphate-buffered saline, pH 7.2) and a 1 μL of $NADP^+$ (24 μ*M*) solution. The final concentrations of protein and compound in each well were 5 and 25 μ*M*, respectively. DMSO/methanol or methanol was used as a background vehicle control at a final concentration of 2.5%–3.0%. Well plates were sealed with a qPCR adhesive seal sheet (4titude, Dorking, UK), centrifuged using a low-speed Flexpin Bench-top Centrifuge (TOMY-LC-220, TOMY, Japan) at 1000 rpm for 1 min to remove air bubbles, and then placed in the RT-PCR instrument. DSF was performed from 25 to 95°C in increments of 1°C per minute. T_m was determined using the software, StepOnePlus or Igor Pro V.6. DSF measurements were repeated at least three times.

CD measurements and analysis

The thermal stabilities of AKR1A1 and AKR1B10 in the absence or presence of various ligands (C12, C18, C21, C26, and $NADP^+$) were investigated using near-UV circular dichroism (CD). The concentrations of the proteins and the ligands used in the experiments were 5 and 25 μ*M*, respectively. Buffers used for CD measurements were 50 m*M* sodium phosphate (pH 7) containing 150 m*M* NaCl, 1 m*M* 2-mercaptoethanol, 0.5 m*M* EDTA, 4% glycerol, and various concentrations of urea (0–9 *M*). A 150-μL fraction of each samples was placed in a quartz cell with the path length of 1 mm, and the ellipticity at 190–260 nm was recorded at 5°C using Chirascan-Plus CD™ spectrometer (Applied Photophysics, Leatherhead, Surrey, UK). Then, the temperature was gradually increased up to 35°C with the rate of 1°C /min, and the change of the ellipticity at 222 nm was recorded every 2.5°C. The ellipticity as a function of urea concentration at the various temperatures was analyzed by assuming a two-state or three-state unfolding mechanism[42] to derive the free-energy difference between the native and unfolded states (ΔG_{UN}). The ΔG_{UN} versus T plot was subsequently analyzed by Gibbs–Helmholtz equation[19,20]

$$\Delta G_{UN} = \Delta H_{vH}\left(1-\frac{T}{T_m}\right) - \Delta C_p\left(T_m - T + T\ \ln\frac{T}{T_m}\right) \quad (2)$$

where ΔH_{vf}, ΔC_p, and T_m represent the van't Hoff enthalpy, isobaric heat capacity change upon the unfolding and melting temperature, respectively. Here, the T_m value was fixed to the values obtained by DSF experiments (see above), and ΔH_{vf}, ΔC_p were determined by a least squares fitting. ΔH and ΔS at arbitrary temperature were calculated according to the following equations.

$$\Delta H(T) = \Delta H_{vH} + \Delta C_p\ (T - T_m) \quad (3)$$

$$\Delta S(T) = \Delta S_{vH} + \Delta C_p \ln T/T_m = \Delta H_{vH}/T_m + \Delta C_p \ln T/T_m \quad (4)$$

The CD measurements and analysis were also performed in the presence of various ligands, and $\Delta\Delta G$, $\Delta\Delta H$ and $\Delta\Delta S$ were calculated by the following equations.

$$\Delta\Delta G = \Delta G_{free} - \Delta G_{ligand} \quad (5)$$

$$\Delta\Delta H = \Delta H_{free} - \Delta H_{ligand} \quad (6)$$

$$\Delta\Delta S = \Delta S_{\text{free}} - \Delta S_{\text{ligand}} \quad (7)$$

The subscripts free and ligand refer to the values in the absence or presence of a ligand, respectively. Of note, in order to simplify the fitting process, the *m*-value and ΔC_p were assumed to be not affected by the presence of ligand, as these two parameters are mainly determined from the change in the solvent-accessible surface area upon unfolding (ΔSASA).[43] Based on the crystal structure of AKR1B10 complex with the Tolrestat (C12) (PDB: 1ZUA), as well as an estimated solvent accessible surface area of the unfolded state,[44] ΔSASA is calculated to be 40,775 and 41,526 Å^2 in the absence and presence of the ligand, respectively, which are almost unchanged by the ligand binding.

APPENDIX: THERMODYNAMIC THEORY ON THE CHANGE IN STABILITY OF THE NATIVE CONFORMATION UPON LIGAND BINDING

In a new system consisting of native state (*N*), intermediate or denatured state (*I*), and ligand (*L*), the following reaction occurs.

$$NL \leftrightarrow N + L \leftrightarrow I + L \leftrightarrow IL \quad (A1)$$

Then, the free energy of stabilization ($\Delta\Delta G$) upon ligand binding is calculated as follows:

$$\Delta\Delta G = RT\left\{\ln\frac{[N]_0}{[I]_0} - \ln\frac{[N]_L + [NL]_L}{[I]_L + [IL]_L}\right\}, \quad K_{dN} = \frac{[N]_L[L]_L}{[NL]_L}, \quad K_{dI} = \frac{[I]_L[L]_L}{[IL]_L} \quad (A2)$$

where $[X]_o$ and $[X]_L$ indicate the population of *X* without and with ligand, respectively. Here we considered $[N]_L$ and $[NL]_L$ to be within the native ensemble, and $[I]_L$ and $[IL]_L$ within the non-native ensemble. Then we can further proceed as follows:

$$[NL]_L = \frac{[N]_L[L]_L}{K_{dN}}, [IL]_L = \frac{[I]_L[L]_L}{K_{dI}},$$
$$\ln\frac{[N]_L + [NL]_L}{[I]_L + [IL]_L} = \ln\frac{[N]_L + \frac{[N]_L[L]_L}{K_{dN}}}{[I]_L + \frac{[I]_L[L]_L}{K_{dI}}} =$$
$$\ln\frac{[N]_L}{[I]_L}\left(\frac{1+\left(\frac{[L]_L}{K_{dN}}\right)}{1+\left(\frac{[L]_L}{K_{dI}}\right)}\right) = \ln\frac{[N]_L}{[I]_L} + \ln\left(\frac{1+\left(\frac{[L]_L}{K_{dN}}\right)}{1+\left(\frac{[L]_L}{K_{dI}}\right)}\right) \quad (A3)$$

Thus, $\Delta\Delta G = RT\ln\frac{[N]_0}{[I]_0} - RT\ln\frac{[N]_L + [NL]_L}{[I]_L + [IL]_L}$

$$= RT\ln\frac{[N]_0}{[I]_0} - RT\ln\frac{[N]_L}{[I]_L} - RT\ln\left(\frac{1+\left(\frac{[L]_L}{K_{dN}}\right)}{1+\left(\frac{[L]_L}{K_{dI}}\right)}\right) \quad (A4)$$

If the free ligand never affects the free energy levels of the native and non-native states, that is, it has no effect on the solvent structure, then

$$\Delta\Delta G = -RT\ln\left(\frac{1+\left(\frac{[L]_L}{K_{dN}}\right)}{1+\left(\frac{[L]_L}{K_{dI}}\right)}\right) \quad (A5)$$

which can be negative (stabilizer chaperone) or positive (destabilizer chaperone) depending on binding constants and also free ligand concentration.

Also we can formulate the melting temperature (T_m) obtained by differential scanning fluorimetry (DSF).[14] In the absence of ligand, for small changes in T_m ($\Delta T_o = T - T_m^0$),

$$\Delta G_{D-N(T)} \sim \left(-\Delta S_{D-N(T)} - \Delta C_{p,D-N(t)} \ln\left(\frac{T}{T_m^0}\right) - T_m^0\Delta C_{p,D-N(t)}\right)\Delta T_o \quad (A6)$$

where $\Delta X_{D\text{-}N(T)} = X_{D(T)} - X_{N(T)}$

While in the presence of ligand, for small changes in T_m ($\Delta T_b = T - T_m^b$),

$$\Delta G_{D-NL(T)} \sim \left(-\Delta S_{D-NL(T)} - \Delta C_{p,D-NL(t)} \ln\left(\frac{T}{T_m^b}\right) - T_m^b\Delta C_{p,D-NL(t)}\right)\Delta T_b \quad (A7)$$

If we define $\Delta\Delta S$ as follows:

$$\Delta\Delta S = \Delta S_{D-N(T)} - \Delta S_{D-NL(T)} \quad (A8)$$

$$\Delta\Delta C_p = \Delta C_{p,\ D-N(T)} - \Delta C_{p,\ D-NL(T)} \quad (A9)$$

$$\Delta\Delta G = -\Delta S_{D-NL(T)}\Delta T_b + \Delta S_{D-N(T)}\Delta T_o - \Delta C_{p,D-NL(t)} \ln\left(\frac{T}{T_m^b}\right)\Delta T_b + \Delta C_{p,D-N(t)}\ln\left(\frac{T}{T_m^0}\right) \Delta T_o - T_m^b\Delta C_{p,\ D-NL(T)}\Delta T_b + T_m^0\Delta C_{p,\ D-N(T)}\Delta T_o \quad (A10)$$

Thus,

$$\Delta S_{D-N(T)} = \Delta S_{D-NL(T)} + \Delta\Delta S \quad (A11)$$

$$\Delta C_{p,D-N(T)} = \Delta C_{p,D-NL(T)} + \Delta\Delta C_p \quad (A12)$$

$$\Delta\Delta G = \Delta S_{D-N(T)}\Delta T_o + \left(-\Delta S_{D-N(T)} - \Delta\Delta S\right)\Delta T_b + \Delta C_{p,D-N(t)} \ln\left(\frac{T}{T_m^0}\right)\Delta T_o - \left(\Delta C_{p,D-N(T)} + \Delta\Delta C_p\right) \ln\left(\frac{T}{T_m^b}\right)\Delta T_b + T_m^0 \Delta C_{p,D-N(T)}\Delta T_o + \left(-T_m^b \Delta C_{p,D-NL(T)} - T_m^b \Delta\Delta C_p\right)\Delta T_b \quad \text{(A13)}$$

Finally, we can obtain the alteration of free energy upon ligand binding as follows:

$$\Delta\Delta G = -\Delta S_{D-N(T)}\Delta T - \Delta\Delta S\Delta T_b + \Delta C_{p,D-N(t)} \left(\ln\left(\frac{T}{T_m^0}\right)\Delta T_o - \ln\left(\frac{T}{T_m^b}\right)\Delta T_b\right) - \Delta\Delta C_p \ln\left(\frac{T}{T_m^b}\right) \Delta T_b + \Delta C_{p,D-N(T)}\left(T\Delta T - \Delta T^2\right) - \Delta\Delta C_p T_m^b \Delta T_b \quad \text{(A14)}$$

in which $\Delta T = T_m^b - T_m^0$, $\Delta T^2 = \left(T_m^b\right)^2 - \left(T_m^0\right)^2$.

Therefore, when $\Delta\Delta C_P$ can be neglected, $\Delta\Delta G$ can be linearly dependent on the temperature with a slope of

$$\frac{\Delta\Delta G}{T} \sim -\Delta\Delta S + \Delta C_{p,D-N(T)}\left(\Delta T + \ln\left(\frac{T_m^b}{T_m^0}\right)\right). \quad \text{(A15)}$$

This additivity generally persists even in case of multiple ligand binding including allosteric effect.

Conflicts of interest

The authors have no conflict of interest directly relevant to the content of this article.

Acknowledgment

We thank Sachie Hori for providing technical help.

References

1. Kuwata K (2013) Logical design of medical chaperone for prion diseases. Curr Top Med Chem 13:2432–2440.
2. Ma B, Yamaguchi K, Fukuoka M, Kuwata K (2016) Logical design of anti-prion agents using NAGARA. Biochem Biophys Res Commun 469.4:930–935.
3. Kamatari Y, Hayano Y, Yamaguchi K-i, Hosokawa-Muto J, Kuwata K (2012) Characterization of anti-prion compounds according to the binding properties to the prion protein. Protein Sci 21:154–154.
4. Kuwata K, Nishida N, Matsumoto T, Kamatari YO, Hosokawa-Muto J, Kodama K, Nakamura HK, Kimura K, Kawasaki M, Takakura Y, Shirabe S, Takata J, Kataoka Y, Katamine S (2007) Hot spots in prion protein for pathogenic conversion. Proc Natl Acad Sci USA 104:11921–11926.
5. Crosas B, Hyndman DJ, Gallego O, Martras S, Pares X, Flynn TG, Farres J (2003) Human aldose reductase and human small intestine aldose reductase are efficient retinal reductases: consequences for retinoid metabolism. Biochem J 373:973–979.
6. Ruiz FX, Gallego O, Ardevol A, Moro A, Dominguez M, Alvarez S, Alvarez R, de Lera AR, Rovira C, Fita I, Pares X, Farres J (2009) Aldo-keto reductases from the AKR1B subfamily: retinoid specificity and control of cellular retinoic acid levels. Chem Biol Interact 178: 171–177.
7. Ma J, Yan R, Zu X, Cheng JM, Rao K, Liao DF, Cao D (2008) Aldo-keto reductase family 1 B10 affects fatty acid synthesis by regulating the stability of acetyl-CoA carboxylase-alpha in breast cancer cells. J Biol Chem 283:3418–3423.
8. Huang L, He R, Luo W, Zhu YS, Li J, Tan T, Zhang X, Hu Z, Luo D (2016) Aldo-keto reductase family 1 member B10 inhibitors: Potential drugs for cancer treatment. Recent Pat Anticancer Drug Discov 11:184–196.
9. Wang C, Yan R, Luo D, Watabe K, Liao DF, Cao D (2009) Aldo-keto reductase family 1 member B10 promotes cell survival by regulating lipid synthesis and eliminating carbonyls. J Biol Chem 284:26742–26748.
10. Endo S, Matsunaga T, Mamiya H, Ohta C, Soda M, Kitade Y, Tajima K, Zhao HT, El-Kabbani O, Hara A (2009) Kinetic studies of AKR1B10, human aldose reductase-like protein: endogenous substrates and inhibition by steroids. Arch Biochem Biophys 487:1–9.
11. Endo S, Hu D, Suyama M, Matsunaga T, Sugimoto K, Matsuya Y, El-Kabbani O, Kuwata K, Hara A, Kitade Y, Toyooka N (2013) Synthesis and structure-activity relationship of 2-phenyliminochromene derivatives as inhibitors for aldo-keto reductase (AKR) 1B10. Bioorg Med Chem 21:6378–6384.
12. Soda M, Hu D, Endo S, Takemura M, Li J, Wada R, Ifuku S, Zhao HT, El-Kabbani O, Ohta S, Yamamura K, Toyooka N, Hara A, Matsunaga T (2012) Design, synthesis and evaluation of caffeic acid phenethyl ester-based inhibitors targeting a selectivity pocket in the active site of human aldo-keto reductase 1B10. Eur J Med Chem 48:321–329.
13. Privalov PL, Gill SJ (1988) Stability of protein structure and hydrophobic interaction. Adv Prot Chem 39:191–234.
14. Brandt T, Kaar JL, Fersht AR, Veprintsev DB (2012) Stability of p53 homologs. PloS One 7:e47889.
15. Kinoshita M (2008) Molecular origin of the hydrophobic effect: analysis using the angle-dependent integral equation theory. J Chem Phys 128:024507.
16. El-Kabbani O, Green NC, Lin G, Carson M, Narayana SV, Moore KM, Flynn TG, DeLucas LJ (1994) Structures of human and porcine aldehyde reductase: an enzyme implicated in diabetic complications. Acta Cryst D50:859–868.
17. Gallego O, Ruiz FX, Ardevol A, Dominguez M, Alvarez R, de Lera AR, Rovira C, Farres J, Fita I, Pares X (2007) Structural basis for the high all-trans-retinaldehyde reductase activity of the tumor marker AKR1B10. Proc Natl Acad Sci USA 104:20764–20769.
18. Santoro MM, Bolen DW (1992) A test of the linear extrapolation of unfolding free energy changes over an extended denaturant concentration range. Biochemistry 31:4901–4907.
19. Pace CN, Laurents DV (1989) A new method for determining the heat capacity change for protein folding. Biochemistry 28:2520–2525.
20. Talla-Singh D, Stites WE (2008) Refinement of noncalorimetric determination of the change in heat capacity, DeltaC(p), of protein unfolding and validation across a wide temperature range. Proteins 71:1607–1616.
21. Koshland DE (1958) Application of a theory of enzyme specificity to protein synthesis. Proc Natl Acad Sci USA 44:98–104.
22. Brandts JF, Lin LN (1990) Study of strong to ultratight protein interactions using differential scanning calorimetry. Biochemistry 29:6927–6940.

23. Murphy KP (2001) Stabilization of protein structure. Methods Mol Biol 168:1–16.
24. Matulis D, Kranz JK, Salemme FR, Todd MJ (2005) Thermodynamic stability of carbonic anhydrase: measurements of binding affinity and stoichiometry using ThermoFluor. Biochemistry 44:5258–5266.
25. Cimmperman P, Baranauskiene L, Jachimoviciute S, Jachno J, Torresan J, Michailoviene V, Matuliene J, Sereikaite J, Bumelis V, Matulis D (2008) A quantitative model of thermal stabilization and destabilization of proteins by ligands. Biophys J 95:3222–3231.
26. Dyson HJ, Wright PE (2004) Unfolded proteins and protein folding studied by NMR. Chem Rev 104:3607–3622.
27. Hilser VJ, Thompson EB (2007) Intrinsic disorder as a mechanism to optimize allosteric coupling in proteins. Proc Natl Acad Sci USA 104:8311–8315.
28. Cohen FE, Kelly JW (2003) Therapeutic approaches to protein-misfolding diseases. Nature 426:905–909.
29. Monod J, Wyman J, Changeux JP (1965) On the nature of allosteric transitions: A plausible model. J Mol Biol 12:88–118.
30. Koshland DE, Jr, Nemethy G, Filmer D (1966) Comparison of experimental binding data and theoretical models in proteins containing subunits. Biochemistry 5:365–385.
31. Palmer AG 3rd (2015) Enzyme dynamics from NMR spectroscopy. Acc Chem Res 48:457–465.
32. Rea AM, Thurston V, Searle MS (2009) Mechanism of ligand-induced folding of a natively unfolded helixless variant of rabbit I-BABP. Biochemistry 48:7556–7564.
33. Bohren KM, Bullock B, Wermuth B, Gabbay KH (1989) The aldo-keto reductase superfamily. cDNAs and deduced amino acid sequences of human aldehyde and aldose reductases. J Biol Chem 264:9547–9551.
34. Cao D, Fan ST, Chung SS (1998) Identification and characterization of a novel human aldose reductase-like gene. J Biol Chem 273:11429–11435.
35. Cremers CM, Knoefler D, Vitvitsky V, Banerjee R, Jakob U (2014) Bile salts act as effective protein-unfolding agents and instigators of disulfide stress in vivo. Proc Natl Acad Sci USA 111:E1610–E1619.
36. Gerbod MC, Janciauskiene S, Jeppsson JO, Eriksson S (1998) The in vitro effect of lithocholic acid on the polymerization properties of PiZ alpha-1-antitrypsin. Arch Biochem Biophys 351:167–174.
37. Beach A, Richard VR, Bourque S, Boukh-Viner T, Kyryakov P, Gomez-Perez A, Arlia-Ciommo A, Feldman R, Leonov A, Piano A, Svistkova V, Titorenko VI (2015) Lithocholic bile acid accumulated in yeast mitochondria orchestrates a development of an anti-aging cellular pattern by causing age-related changes in cellular proteome. Cell Cycle 14:1643–1656.
38. Andreotti G, Citro V, Correra A, Cubellis MV (2014) A thermodynamic assay to test pharmacological chaperones for Fabry disease. Biochim Biophys Acta 1840: 1214–1224.
39. Siekierska A, De Baets G, Reumers J, Gallardo R, Rudyak S, Broersen K, Couceiro J, Van Durme J, Schymkowitz J, Rousseau F (2012) Alpha-Galactosidase aggregation is a determinant of pharmacological chaperone efficacy on Fabry disease mutants. J Biol Chem 287:28386–28397.
40. Hosokawa-Muto J, Kamatari YO, Nakamura HK, Kuwata K (2009) Variety of antiprion compounds discovered through an in silico screen based on cellular-form prion protein structure: Correlation between antiprion activity and binding affinity. Antimicrob Agents Chemother 53:765–771.
41. Niesen FH, Berglund H, Vedadi M (2007) The use of differential scanning fluorimetry to detect ligand interactions that promote protein stability. Nat Protoc 2: 2212–2221.
42. Latypov RF, Cheng H, Roder NA, Zhang J, Roder H (2006) Structural characterization of an equilibrium unfolding intermediate in cytochrome c. J Mol Biol 357:1009–1025.
43. Myers JK, Pace CN, Scholtz JM (1995) Denaturant m values and heat capacity changes: relation to changes in accessible surface areas of protein unfolding. Protein Sci 4:2138–2148.
44. Creamer TP, Srinivasan R, Rose GD (1995) Modeling unfolded states of peptides and proteins. Biochemistry 34:16245–16250.